CLM - R 12

United Kingdom Atomic Energy Authority

RESEARCH GROUP

Report

PLASMA CONFINEMENT USING ROTATING MAGNETIC FIELDS

H. BLEVIN P. C. THONEMANN

Culham Laboratory,

Culham, Abingdon, Berks.

1961

Available from H.M. Stationery Office
FOUR SHILLINGS NET

U.D.C.
621.039.629

UNCLASSIFIED
(Approved for Sale)

CLM - R 12

PLASMA CONFINEMENT USING ROTATING MAGNETIC FIELDS

by

H. Blevin
P.C. Thonemann

ABSTRACT

An investigation has been made of the current distribution set up by a magnetic field rotating about the axis of a cylindrical plasma. If the plasma resistivity was sufficiently small electrons rotate with the magnetic field producing a steady azimuthal current. In conjunction with an externally applied axial magnetic field such a system can be used to confine plasma away from the walls of a discharge tube. Experiments are described in which the radial density distribution was measured and compared with that calculated from theory.

Culham Laboratory,
Atomic Energy Research Establishment,
HARWELL
Berks.

October, 1961

HL61/5072 (C.18)
/PMF

CONTENTS

TABLES

ILLUSTRATIONS

1. Introduction

A plasma with sufficiently high conductivity behaves as though it were "frozen" to lines of magnetic force. In order that the plasma closely follows the "motion" of a periodically varying magnetic field both the electron and ion cyclotron frequencies must be much greater than the frequency at which the magnetic field changes.

If the frequency of the magnetic field variation lies between the ion and electron cyclotron frequencies then electrons tend to be "frozen" to the lines of force whereas ions are not. In most circumstances differential motion of electrons and ions resulting from a perturbation of the magnetic field is prevented by space charge electric fields. However, if the lines of force "move" in a direction parallel to a closed surface of constant charge density no charge separation takes place and the magnetic field carries the electrons with it. It is possible, therefore, to produce steady electrical currents in a plasma by using "moving" magnetic fields. This phenomena has been demonstrated experimentally by Thonemann, Cowhig and Devenport (1).

If the plasma is completely isolated, collisions between electrons and ions will eventually bring both charges to the same velocity and all currents vanish. In laboratory plasmas momentum transfer to the walls of the vessel either by charge exchange or by the direct impact of ions ensures the maintenance of such currents.

In the experiments described here a magnetic field "rotates" about the axis of a cylindrical plasma in a manner similar to the fields in an induction motor. When the conductivity is sufficiently high electrons rotate about the axis and azimuthal currents up to 750 amperes per centimeter length have been observed. In the presence of an externally applied axial magnetic field the plasma can be collapsed towards the axis until the radial component of the Lorentz force is balanced by the plasma pressure gradient.

2. Nomenclature

Electromagnetic units are used.

r, θ, z	cylindrical co-ordinates.
E	electric field
B	magnetic induction
J	current density
n	electron density
N_o	electron line density
N	electron line density outside a cylinder of radius r.
η	resistivity

ω	angular frequency of rotating magnetic field
ω_i, ω_e	ion and electron cyclotron frequencies
p	gas pressure
T_i, T_e	ion and electron temperatures
T	$T = T_i + T_e$
m, M	electron and ion masses.

3. Theory

(i) Current distribution in the plasma.

Consider a cylindrical plasma of infinite length bounded radially by an insulating wall. To this plasma cylinder is applied a transverse magnetic field which rotates about the cylinder axis. The angular frequency ω of the rotating field is such that $\omega_i \ll \omega \ll \omega_e$. The following assumptions are made.

(a) The positive ions are so massive that their motion in the alternating fields can be neglected.

(b) All quantities are independent of the axial co-ordinate.

(c) The electron temperature is constant in space and time.

(d) The plasma is sufficiently highly ionized so that the electrical resistivity is determined by electron-ion collisions.

(e) The currents in the plasma do not distort the applied rotating field to any significant extent.

The equation of electron motion

$$\tilde{E} - \frac{\tilde{J}\times\tilde{B}}{ne} + \frac{\tilde{\nabla}p_e}{ne} - J = 0 \qquad \ldots\ldots\ldots (1),$$

together with an applied field of the form

$$\left.\begin{aligned} B_r &= B_o \cos(\omega t - \theta), \\ B_\theta &= B_o \sin(\omega t - \theta), \\ B_z &= B_a, \end{aligned}\right\}$$

are to be solved for the electron current J.

When $\eta = 0$, these equations have the solution

$$J_\theta = -ner\omega$$
$$J_r = 0$$
$$J_z = 0 \qquad \ldots\ldots\ldots (2),$$

and electrons are "frozen" to the rotating lines of force.

When $\eta \neq 0$, and assuming $J_r = 0$, then

$$J_\theta = \frac{ner\omega}{1 + \frac{2(ne\eta)^2}{B_o^2}},$$

$$J_z = -\frac{2ne\eta J_\theta}{B_o} \cos(\omega t - \theta).$$

The presence of an axial current tends to attenuate the rotating field at the axis and also produces a phase shift in the field at the axis with respect to that at the plasma boundary. In order that this effect should be small it is necessary that $2(ne\eta)^2/B_o^2 \ll 1$ in which case electrons rotate in synchronism with the rotating field and there is negligible "slip". This condition states that electrons should be able to spiral many times about the rotating field vector without undergoing collisions.

Ion Motion

If the frequency of the rotating field lies well above ω_i the induced ion currents are very much smaller than the electron currents. However, ions are eventually set into rotation by electron-ion collisions and in a completely isolated plasma both ions and electrons must ultimately rotate synchronously with the field. The characteristic time for this rotation is $B_o/ne\eta\omega_i$. In the experiments to be described a heavy gas was chosen so that the time for ions to gain appreciable azimuthal velocity was much longer than the observation time.

In practical cases the loss of momentum by charge exchange or by ions hitting the wall will ensure a nett current flow. If the predominant loss is due to charge exchange the equilibrium ion velocity can be calculated. Thus

$$e\eta J_\theta = MV\nu ,$$

where V is the ion velocity and ν is the charge-exchange collision frequency. Thus $ne^2\eta(v - V) = MVn_o(\overline{\sigma V})$, where v is the electron azimuthal velocity, n_o is the neutral gas density, and is the charge-exchange cross-section.

Therefore $\frac{V}{v} = \frac{1}{1 + M \frac{n_o}{n_i} \frac{\overline{\sigma V}}{e^2 \eta}}$

For $V \ll v$ it is required that

$$\frac{n_o}{n_i} \gg \frac{e^2 n}{M(\overline{\sigma V})} .$$

(ii) Equilibrium Radial Density Distribution

The azimuthal electron current produces an axial field which drives the plasma radially outwards. If an externally produced axial magnetic field B_a is superimposed in a direction opposite to the self field, the plasma is driven towards the axis until the plasma pressure gradient balances the inward Lorentz force.

Thus $kT \frac{dn}{dr} = J_\theta B_z + nmr\omega^2 \qquad T = T_i + T_e .$

$$= - ner\omega \; B_a - 4\pi e\omega \int_r^\infty nrdr + nmr\omega^2 .$$

The centrifugal term can be neglected provided $\frac{eBa}{m} \gg$, and it is then possible to solve for $n = f(r)$.

Putting $N = 2\pi \int_r^\infty nrdr$, that is, the number of electrons per unit length outside a cylinder of radius r, it follows that

$$\frac{dN}{dr} = 2\pi nr,$$

$$\text{and } N = \frac{B_a}{e\omega} \left[1 + \left(\frac{B_a}{N_o e\omega} - 1 \right) \exp\left(\frac{B_a e\omega}{2kT} r^2 \right) \right]^{-1} ,$$

where N_o is the electron line density.

It then follows immediately that

$$n = \frac{B_a^2}{2\pi kT} \frac{\left(\frac{B_a}{N_o e\omega} - 1 \right) \exp\left(\frac{B_a e\omega}{2kT} r^2 \right)}{\left[1 + \left(\frac{B_a}{N_o e\omega} - 1 \right) \exp\left(\frac{B_a e\omega}{2kT} r^2 \right) \right]^2} \qquad \ldots\ldots\ldots (3),$$

The axial magnetic field as a function of radius is given by

$$B_z = B_a - 2N e\omega,$$

$$\text{or } B_z/B_a = \frac{\left(\frac{B_a}{N_o e\omega} - 1\right)\exp\left(\frac{B_a e\omega}{2kT} r^2\right) - 1}{\left(\frac{B_a}{N_o e\omega} - 1\right)\exp\left(\frac{B_a e\omega}{2kT} r^2\right) + 1} \qquad \ldots\ldots\ldots (4),$$

Equations (3) and (4) are valid for an unbounded plasma but may be used for a bounded plasma without significant error provided $n_{wall} << n_{axis}$.

There are three special cases of interest.

(a) If $\frac{B_a}{N_o e\omega} > 2$, n decreases monotonically with increasing radius and the axial field is unidirectional.

(b) If $1 < \frac{B_a}{N_o e\omega} < 2$, n is a maximum and $B_z = 0$ when

$$r = \frac{2kT}{B_a e\omega} \ln \frac{N_o e\omega}{\left(B_a - N_o e\omega\right)}\Bigg]^{\frac{1}{2}}.$$ At smaller values of radius the axial field is reversed.

(c) If $\frac{B_a}{N_o e\omega} < 1$ the reverse field is greater than B_c and the plasma cannot be confined.

Effect of conducting wall at radius R.

The current in the wall produces an axial field B_1 so that the total axial flux is conserved.

$$B_1 = \frac{8\pi}{R^2}\left[\int_o^R \left(\int_r^R nrdr\right) rdr\right], \text{ where it is assumed that the plasma density}$$

at the wall is small. Then

$$N = \frac{B^*}{e\omega}\left[1 + \left(\frac{B^*}{N_o e\omega} - 1\right)\exp\left(\frac{B^* e\omega}{2kT} r^2\right)\right]^{-1},$$

where $B^* = B_a + B_1$.

The presence of the conducting wall improves the confinement of plasma away from the walls, effectively increasing the applied field B_a to a value B^* given by

$$B^* = B_a + \frac{4kT}{e\omega R^2}\,\ell n\left(\frac{B^*}{B^* - N_o e\omega}\right)$$

(iii) Power dissipated by Joule heating

The power dissipated per unit length in an annulus of thickness dr and of radius r is

$$dP = \eta(J_\theta + J_z^2)\,2\pi r\,dr$$

$$= \eta\left[1 + 2\left(\frac{ne\eta}{B_o}\right)^2\right] J_\theta^2\,2\pi r\,dr.$$

For $2\left(\frac{ne\eta}{B_o}\right)^2 \ll 1$ corresponding to the experimental conditions with which we are concerned, $J_\theta = -ner\omega$ and

$$dP = \eta(ner\omega)^2\,2\pi r\,dr.$$

Using equation (3) for the electron density distribution and integrating over the radius, the power dissipated per unit length of the plasma column is

$$P = -\eta\,\frac{B_a^2}{6\pi}\left[\frac{\frac{B_a}{N_o e\omega} - 1}{\frac{B_a^2}{(N_o e\omega)^2}} + \ell n\left(1 - \frac{N_o e\omega}{B_a}\right)\right]$$

Putting $F_1\left(\frac{B_a}{N_o e\omega}\right) = -\left[\frac{\frac{B_a}{N_o e\omega} - 1}{\frac{B_a^2}{(N_o e\omega)^2}} + \ell n\left(1 - \frac{N_o e\omega}{B_a}\right)\right]$, then

$$P = \eta\,\frac{B_a^2}{6\pi} \times 10^{-7} F_1\left(\frac{B_a}{N_o e\omega}\right) \text{ watts/cm.}$$

Fig. 1(a) shows $\eta\frac{B_a}{6\pi} \times 10^{-7}$ as a function of electron temperature for several values of the applied axial field B_a. Fig. 1(b) shows the function $F_1\left(\frac{B_a}{N_o e\omega}\right)$. If the plasma temperature is known the power dissipation can be determined from these graphs.

Power balance

An estimate of the electron temperature can be made assuming that the dominant energy loss is by particle loss to the walls.

The power lost to the walls is $n_{wall}\sqrt{\frac{kT_e}{M}}\left(7KT_e + \phi\right) \times 10^{-7}$ watts cm^{-2}

where ϕ is the energy required to produce an ion pair in the plasma and is in general about 100 eV. The factor $7kT_e$ accounts for the energy of an electron and ion pair reaching the wall; the energy of an ion accelerated through the sheath region depends upon the ion mass and the figure used here is an approximation for heavy ions.

Equating the power loss to the walls to the power input enables an expression for the equilibrium electron temperature to be found. Thus

$$T_e^2\left(7kT_e + \phi\right) = \frac{4.6 \times 10^7 \sqrt{A}\, B_a^2}{R\, n_{wall}} F_1\left(\frac{B_a}{N_o e\omega}\right) \qquad \ldots\ldots\ldots (5),$$

where A is the atomic weight and R the radius of the walls.

Now for a well confined plasma equation (3) gives

$$n_{wall} \propto \frac{B_a^2}{2\pi kT}\left(\frac{B_a}{N_o e\omega} - 1\right)^{-1} \exp\left(-\frac{B_a e\omega}{2kT} R^2\right) \qquad \ldots\ldots\ldots (6),$$

Equations (5) and (6) can now be solved for the electron temperature if an assumption is made about the ion temperature.
For example if $T_i = T_e$, then

$$T_e = 2.9 \times 10^{-5} B_a R^2 \omega \left(\ell n \left[\frac{1.2 \times 10^{-5} Te (7kT_e + \phi) R}{M^{\frac{1}{2}} \left(\frac{B_a}{N_o e\omega} - 1\right) F_1\left(\frac{B_a}{N_o e\omega}\right)} \right] \right)^{-1}$$

(iv) Twisting of Rotating Field Lines of Force

For a plasma of finite conductivity, axial currents flow and distort the rotating field lines. The axial current has been calculated in 3(i). It is given by

$$J_z = 2 \frac{ne\eta}{B_o} \frac{ner\omega \cos(\omega t - \theta)}{\left[1 + 2(ne\eta)^2/B_o^2\right]}.$$

The axial electric field is $E_z = B_o r\omega \cos(t - \theta)$ so that the apparent resistivity in the axial direction is

$$\eta^1 = \eta\left(1 + \frac{B_o^2}{2(ne\eta)^2}\right).$$

The phase shift produced in the rotating field at the axis by the presence of these axial currents can be calculated assuming η^1 is independent of radius. This assumption implies firstly that the electron density distribution can be approximated by a rectangular distribution function and secondly that the magnetic field B_o is only slightly attenuated in the plasma interior, which is true provided $2(ne\eta)^2/B_o^2 \ll 1$, i.e. for small axial currents and small phase shifts in the rotating field.

The vector potential $\tilde{A}$ of the rotating field satisfies the equation

$$\nabla^2\tilde{A} = \frac{4\pi}{\eta^1}\frac{\partial\tilde{A}}{\partial t} \quad , \text{ where A has only an axial component.}$$

The solution of this equation outside the plasma column is

$$A_o = B_o\ r + \left(\frac{ber_2x + i\ bei_2x}{ber_ox + i\ bei_ox}\right)\frac{a^2}{r}\ e^{i(\omega t - \theta)}$$

and inside the plasma

$$A_i = \frac{2\ B_o}{i\pi 4\omega\ \eta'}\ \frac{bei_1y - i\ ber_1y}{ber_ox + i\ bei_ox}\ e^{\,i(\omega t - \theta)}$$

where $x = \sqrt{\frac{4\pi\omega}{\eta'}}\ a$, a is the radius of the plasma cylinder and

$$y = \frac{4\pi\omega}{\eta'}\ r\ .$$

The phase shift α in the rotating field at the axis is given by

$$\tan\alpha = \frac{bei_ox}{ber_ox}\ . \qquad \ldots\ldots\ldots\ (7).$$

A measurement of α at the plasma axis enables η' and consequently η to be estimated provided the phase shift and attenuation of the rotating field are small. Figure 2 shows a sketch of the lines of force when there is a 180^o phase shift in the rotating field at the axis. Although such large shifts are observed experimentally they are not suitable for the calculation of plasma resistivity since the field strength is markedly dependent on the radial co-ordinate.

4. Experimental Results.

The experimental conditions were determined by the plasma resistivity η, the gas pressure at which a well ionized plasma can be produced readily, and the

requirement that the frequency of the alternating field should lie between the electron and ion gyrefrequencies in this field. Assuming an electron temperature of 40,000°K, a singly ionized gas, and an initial gas pressure of 10^{-2} mm Hg, the condition $ne\eta/B_o < 1$ requires $B_o > 100$ gauss. The gyrofrequency of a singly charged helium ion in a field of 100 gauss is about 4×10^4 cycles/second so that frequencies in the range 1 - 10 Mc/second are suitable. In most cases argon and xenon were used so that ion rotational effects could be neglected.

The production of magnetic fields of 100 gauss in the megacycle frequency range is a matter of some difficulty if continuous operation is envisaged. However, it is a simple matter to produce such fields by the transient discharge of a condenser in an oscillatory circuit and this latter method was adopted.

The electrical circuit and arrangement of the apparatus is shown in Figure 3. Two capacitors C_1 and C_2 (.04μfd) were charged to 20 kilovolts and discharged $\pi/2$ out of phase through conductors which passed parallel to the axis of a pyrex discharge tube. The spark gap S_1 was adjusted to break down at a predetermined voltage and the spark gap S_2 then triggered half a period later by means of the delay cable D. The two inductances L_1 and L_2 were adjusted to minimise the mutual inductance.

Several discharge tubes were used with diameters from 3 to 5 cm. and about 20 cm. in length. The frequencies used were in the range 1 - 1.5 Mc/second and in the absence of a discharge the circuit current decayed almost linearly to zero in about 30 cycles. The Q of the resonant circuit without spark gaps was several hundred so that the rapid decrement was due to spark gap losses.

A re-entrant tube T, 3 millimeters in diameter and placed diametrically across the discharge tube permitted a variety of probes to be inserted to measure the local magnetic fields. Flux coils F encircled the discharge tube and together with a suitable integrating circuit served to determine the change in the total axial magnetic flux at different positions along the tube. A continuous flow of gas was maintained through the tube and the gas pressure measured by a Pirani gauge.

The magnetic probes inevitably gave a signal at the frequency of the rotating field due to misalignment and electrostatic interference, so that low pass filters with a cut-off frequency of 1.0 mc/sec. were used to eliminate this interference when the steady axial field was being measured.

(ii) Measurements

Table I summarizes the typical parameters found in these experiments. Figure 4 shows typical oscillograph records of magnetic probe measurements. In all cases the upper trace is the applied rotating field measured external to the discharge tube. Figures 4(a), (b), (c) show the axial magnetic field produced at the axis by the azimuthal current. In Figure 4(a) the externally applied axial field is in such a direction as to confine the plasma and the azimuthal current remains constant until the rotating field has decayed to a value where it is screened from the interior of the plasma, (c.f. Figure 4(d)).

Figures 4(b), (c) show the decay in the axial field when no axial field is applied or is in the reverse direction to that needed for confinement. This decay is attributed to the expansion of the plasma to the walls and a subsequent drop in plasma density and temperature due to wall recombination.

At low gas pressures ($\sim 10^{-3}$ mm Hg) the rotating field was not able to ionize the gas efficiently and preionization was required. This was achieved by discharging a small condenser bank (.01μFd, 20 KV) into four single turn coils placed in parallel around the tube, the resonant frequency being 4 Mc/sec. The azimuthal current produced by the rotating field at these low densities persisted for much longer times than previously observed due to the smaller damping on the resonant circuit together with the fact that complete penetration of the rotating field was observed for smaller values of B_0 than found earlier. (c.f. Fig. 5).

Measurements of the axial magnetic field as a function of radius are shown in Figures 6(A), (B). These results were obtained during that period of the discharge when the rotating field penetrated the plasma with a negligible amount of phase shift so that $ne\eta/B \ll 1$ and equations (3) and (4) are applicable. The value of B_z for $r = 0$ gives a direct determination of the line density N_0 and by fitting equation (4) to the measured magnetic field profile the plasma temperature T is determined. This enables n to be calculated as a function of radius from equation (3). These density profiles are also shown in Figs. 6(A), (B). Figure 6(A) corresponds to the case $B_a/N_0 e\omega > 2$ and the electron density has its maximum value on the axis. Figure 6(B) corresponds to the case for which $1 < B/N\ e\omega < 2$ and the axial field is reversed at the axis.

Electron densities have been measured independently by double Langmuir probes in the afterglow period of the discharge and agree with the magnetic probe results within a factor of two. Some typical probe measurements are shown in Figures 7 and 8. However, the temperatures derived from the pressure balance method outlined above are considerably higher than those expected from the power balance relation (equation (5)) and higher than those calculated from

(i) the twisting of magnetic lines of force

(ii) the decay rate of the axial magnetic field.

Both these methods give values for T_e about $4 - 6 \times 10^4$ oK.

This discrepancy can be accounted for by considering the pressure exerted by the rotating magnetic field. In the absence of plasma the amplitude of the rotating field at the axis was about twice that at the walls due to the non-uniformity of the applied field across the tube diameter where the probes were located. In the presence of plasma the amplitude of the rotating field at the axis was often five times that at the walls. The magnetic pressure resulting from this excess field was comparable with the plasma pressure. This "inverse skin effect" could arise from end effects in the following manner. Radial currents at the tube ends interact with the B_z field and produce J_z current in such a phase as to enhance the rotating field at the axis and decrease it near the walls. The probe measurements shown in Figure 4(d) indicate this enhancement of the rotating field at the axis in the early stages of the discharge pulse. This example shows an actual growth of the rotating field

strength at the axis but in many cases the enhancement is only seen through the difference between the decay rates of the rotating field at the axis and at the walls.

Towards the end of the discharge pulse when the rotating field has decayed to a small value such that $2(ne\eta)B_0 \simeq 1$ a marked phase shift is observed in the rotating field at the axis. Figure 9 shows an example of the gradual phase change as the applied field decays in amplitude. Phase shifts of 180° are often observed when the rotating magnetic field decayed to small amplitude (c.f. Figures 4(d), (f).).

The axial field measured at the axis of the tube remains substantially steady throughout the major part of the discharge pulse until the rotating field is screened from the plasma. However, probes situated off-axis show a slow variation in the axial field, Figure 10. The signals from probes on opposite sides of the axis are in phase and the variation of the measured axial field was interpreted as a series of contractions and expansions of the plasma.

Since $B = B_a - 2Ne\omega$, the results indicate that the line density N_0 is constant, while the line density outside a cylinder of radius r is varying. This pulsation of the discharge appears to be associated with the occurance of a high frequency axial field, the frequency of oscillation being the second harmonic of the rotating field. The B_z magnetic probe signals were usually observed after passing through a low pass filter and only the steady field component was used in calculations of electron density distributions. Figure 11 shows the high frequency component of the axial magnetic field at the tube axis, observed by using a high pass filter in the probe circuit. It is noticed that the amplitude of this component varies considerably throughout the pulse and there appears to be a correlation between the amplitude of the second harmonic and the radial density fluctuations. The origin of this high frequency oscillation is not fully understood, but since the total axial flux is also observed to have a high frequency component it would appear that a resonance oscillation of the plasma is involved. In this way the magnetic field perturbation vector could be changing in space but constant in amplitude. Electrons carried with the perturbation would see a constant field and in this way it is possible to have a change in the total axial flux at these high frequencies. The amplitude of the high frequency axial field on the tube axis is dependent on gas pressure but may be as much as 50% of the steady component produced by currents in the plasma.

5. Conclusion

It has been shown that a magnetic field rotating about the axis of a cylindrical plasma produced large azimuthal currents, and in the presence of an external axial magnetic field a plasma can be confined. However, an accurate comparison with theory was not possible in these experiments due to the complications arising from end effects and resonance oscillations in the plasma. Both these phenomena require further investigations in order that their effect can be included in the pressure balance relation. The hydromagnetic stability of the plasma could not be investigated as the confinement tune was too short for such instabilities to grow.

References

Thonemann, P.C., Cowhig, W.T. and Davenport, P.A., Nature 169, 34, (1952).

Davenport, P.A., Ph. D. Thesis, Oxford University (1954).

TABLE I

Gas	P (mm. Hg.)	Tube Diam. (cm.)		B_a (gauss)	B_o (initial value)	$B_a - B_z$	Initial Line density Gas atoms (N_g)	Line density of electrons (N_o)
Xenon	5×10^{-3}	4.9	7.9×10^{6}	730	460	970	4.1×10^{15}	3.9×10^{15}
Xenon	12×10^{-3}	3.3	7.9×10^{6}	650	600	333	3.7×10^{15}	1.3×10^{15}
Argon	14×10^{-3}	3.3	7.9×10^{6}	0	870	870	4.4×10^{15}	3.5×10^{15}
Xenon	3.1×10^{-3}	3.3	5.5×10^{6}	550	420	370	0.94×10^{15}	2.1×10^{15}

Legend for Figures

Figure 1(a) Power dissipation by Joule heating (used in conjunction with Figure 1(b)).

Figure 1(b) Power dissipation by Joule heating (used in conjunction with Figure 1(a).

Figure 2 Twisting of rotating field lines of force in a resistive cylinder.

Figure 3 Apparatus and circuit diagram.

Figure 4 Magnetic probe measurements.

Xenon $p = 3.3 \times 10^{-3}$ mm Ng.

Upper trace - applied rotating field 1 μsec/cm.

Lower trace - axial probe 500 gauss/cm.

(a) B_z field $B_a = +660$ gauss.

(b) " $B_a = 0$ "

(c) " $B_a = -660$ "

(d) rotating field $B_a = +660$ "

(e) " $B_a = 0$ "

(f) " $B_a = -660$ "

Figure 5 Magnetic probe measurements with preionization.

Xenon $p = 2 \times 10^{-3}$ mm Hg.

B = 650 gauss

2 μ sec/cm.

Upper trace - external rotating field.

Lower trace - B_z field at axis 180 gauss/cm.

Figure 6(A) Example of magnetic field profile.

Figure 6(B) Example of magnetic field profile.

Figure 7 Langmuir double probe measurements.

Figure 8 Langmuir double probe measurements.

Legends

Figure 9 Phase shift in rotating field at axis. 1 μ sec/cm.

Upper trace - wall probe.

Lower trace - axial probe.

Figure 10 Axial field measurements.

Argon $p = 3.6 \times 10^{-3}$ mm Hg.

$B_a = 520$ gauss

2 μ sec/cm.

Upper trace - probe at axis 300 gauss/cm.

Lower trace - probe 1 cm. off axis 150 gauss/cm.

(tube diameter = 3.3 cm.)

Figure 11 Second harmonic component of axial field.

Xenon $p = 2.8 \times 10^{-3}$ mm Hg.

$B_a = 690$ gauss

2 μsec/cm.

Upper trace - probe 1 cm. off axis, low frequency pass filter.

Lower trace - probe at axis, high pass filter.

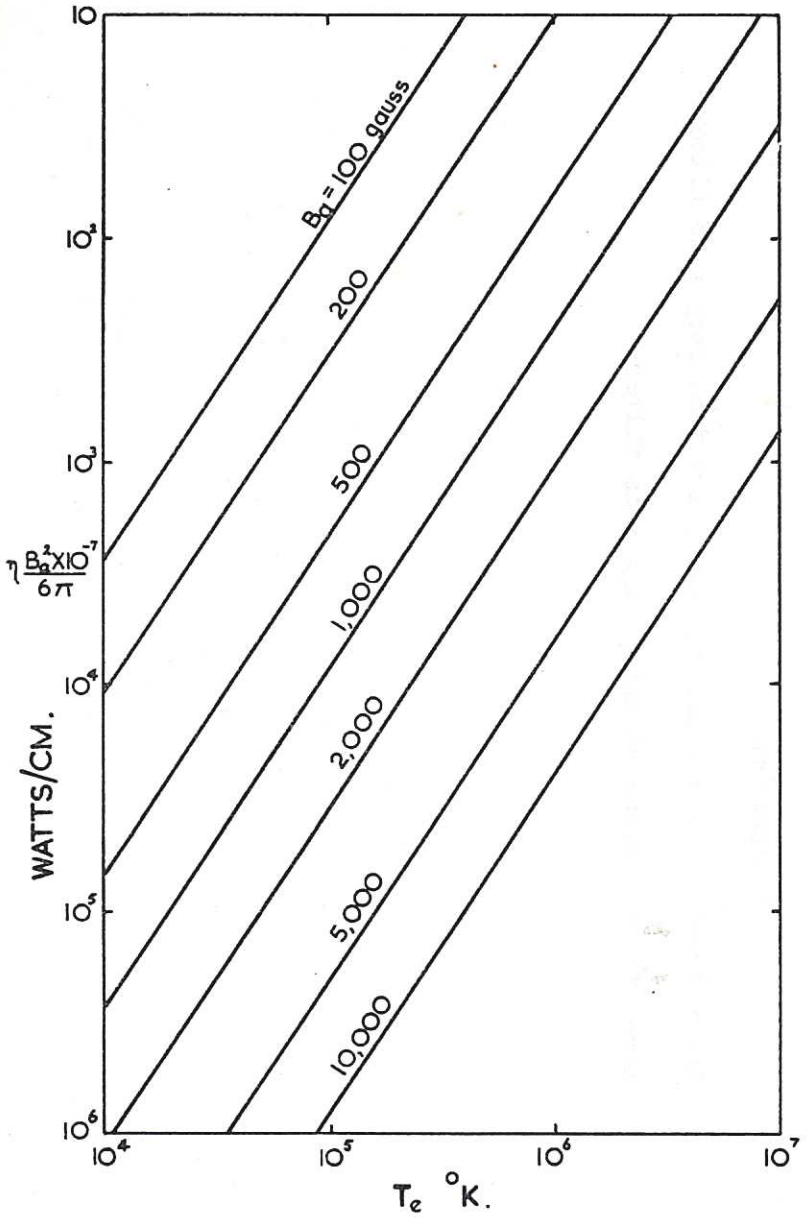

Fig. 1(a).
Power dissipation curves (in conjunction with Fig. 1(b)).

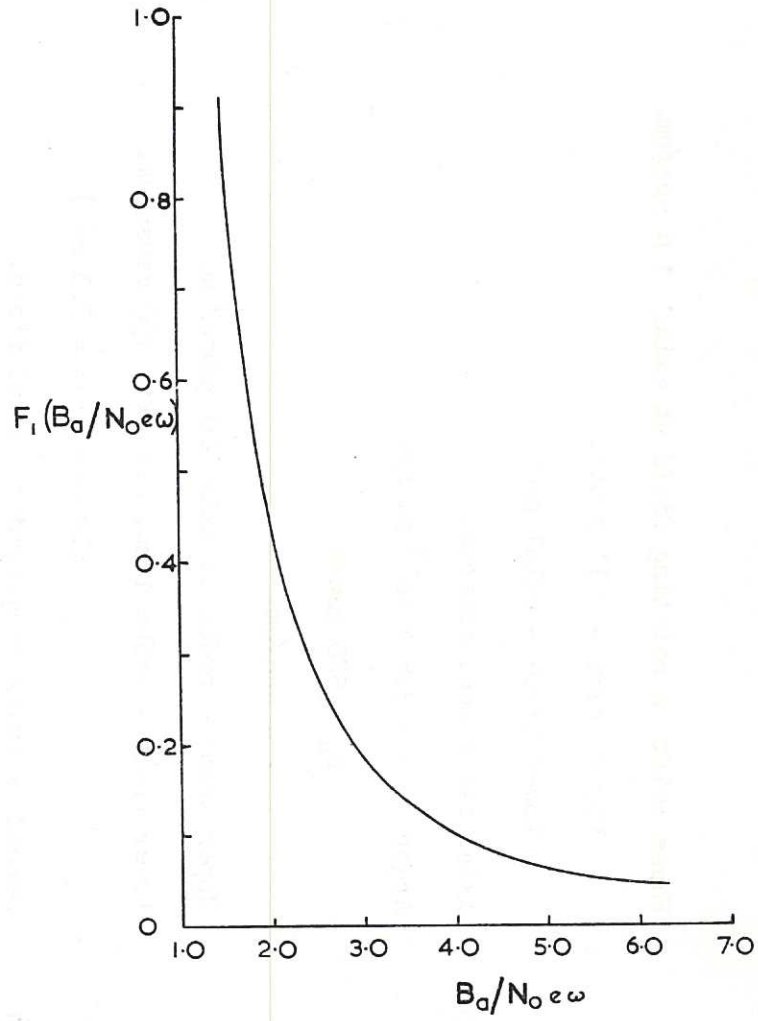

Fig. 1(b).
Power dissipation curves (in conjunction with Fig. 1(a)).

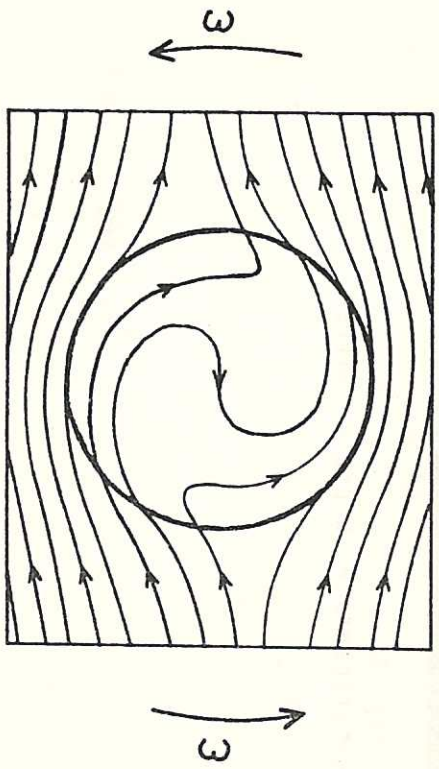

Sketch showing twist in magnetic field rotating about the axis of a cylindrical conductor. Frequency, resistivity and radius chosen to give 180° phase shift at axis.

Fig. 2.
Twisting of rotating field lines of force in a resistive cylinder.

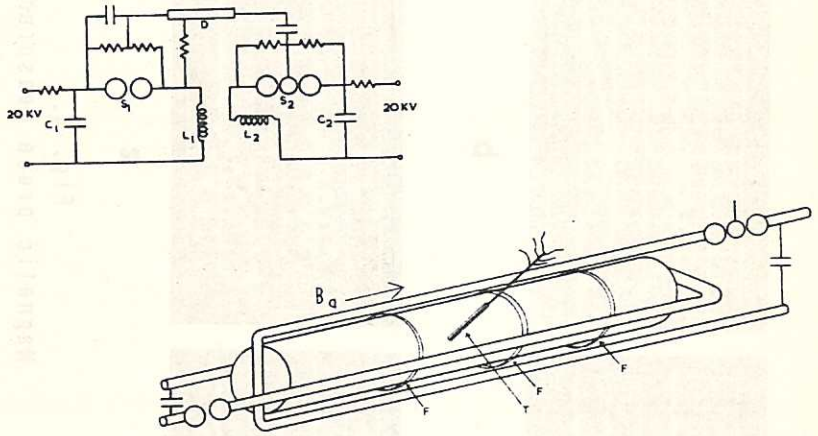

Fig. 3.
Apparatus and circuit diagrams

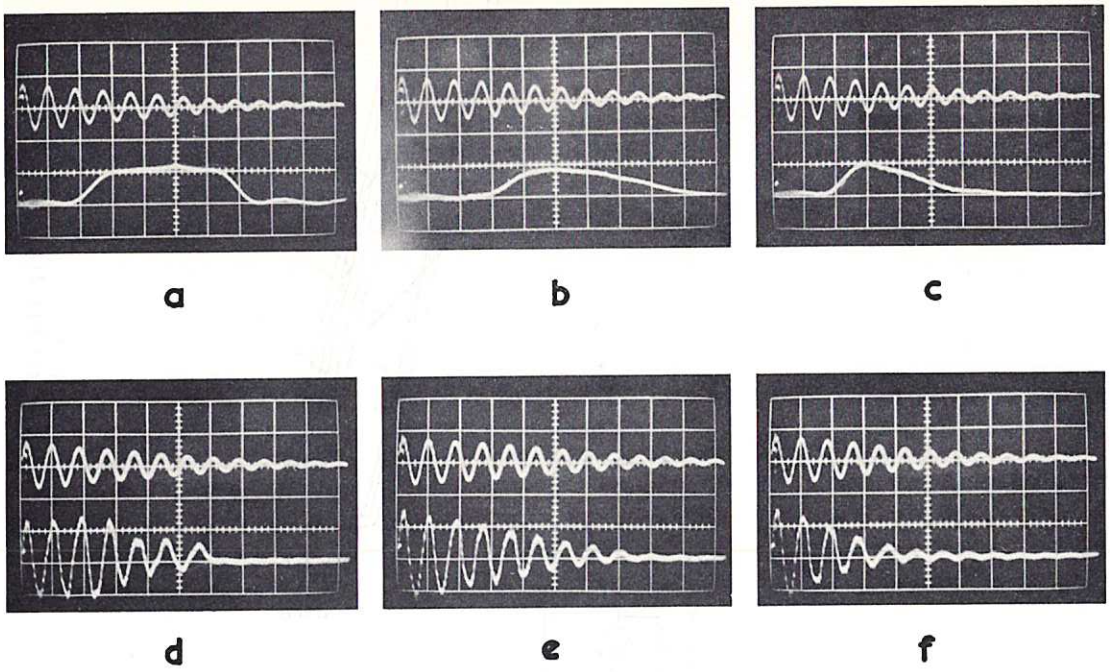

Fig. 4.
Magnetic probe measurements.

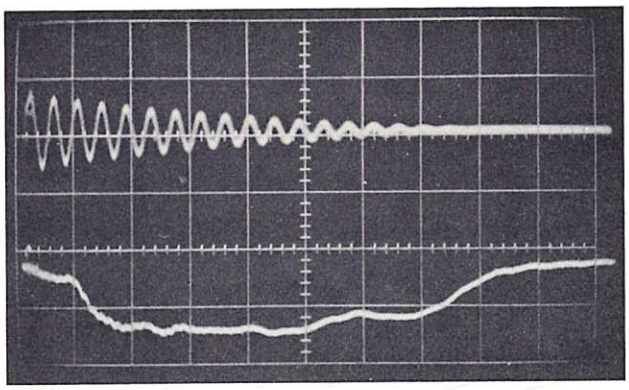

Fig. 5.
Magnetic probe measurements with preionization

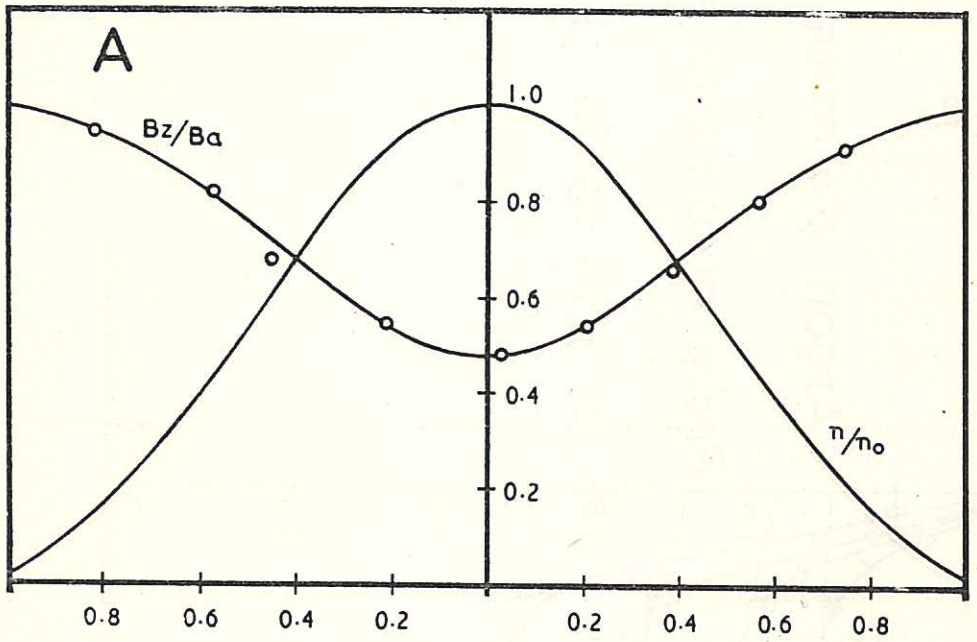

XENON. $p = 1.2 \times 10^{-2}$ mm Hg

$B_a = 650$ gauss

$n_o = 4.4 \times 10^{14}$/cc $\quad T_i + T_e = 2.1 \times 10^5$°K

$N_o = 1.3 \times 10^{15}$/cm

Experimental points o at 6 μ sec

Fig. 6(A).
Examples of magnetic field profile

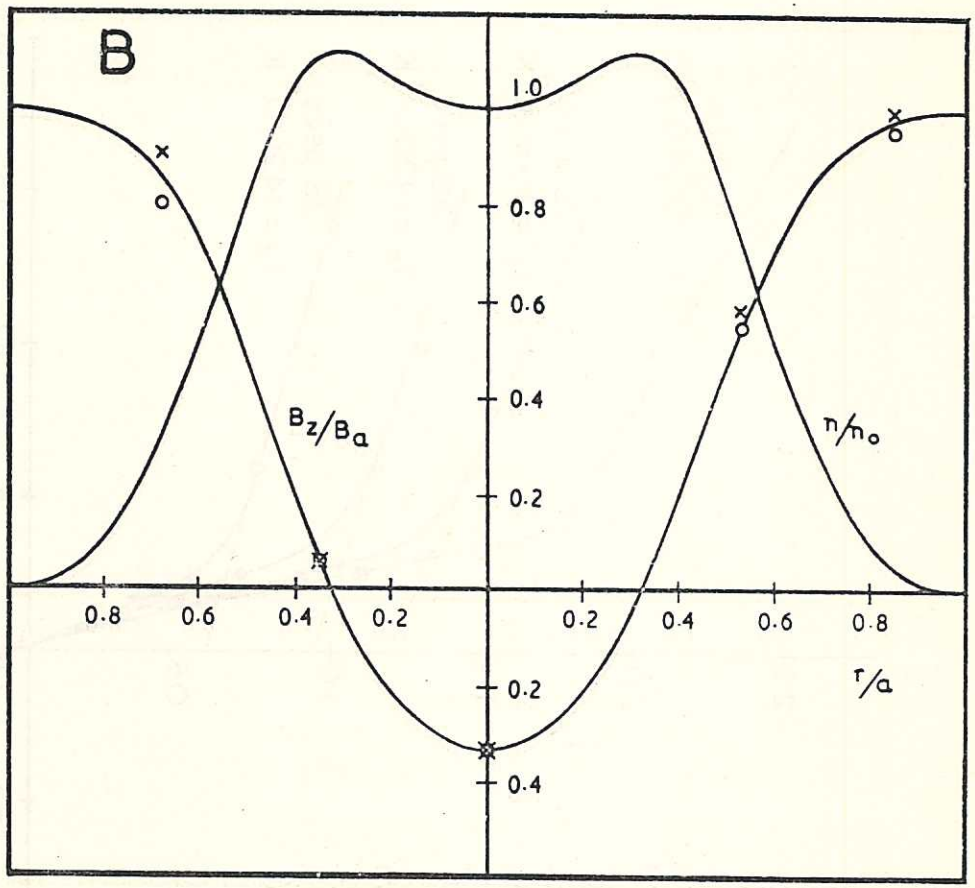

XENON. $p = 5 \times 10^{-3}$ mm Hg.

$B_a = 730$ gauss

$n_o = 4.1 \times 10^{14}$/cc

$N_o = 3.8 \times 10^{15}$/cm

$T_i + T_e = 2.8 \times 10^5$°K

Experimental points

o at 3μ sec

x at 2.5 and 4μ sec

Fig. 6(B).
Example of magnetic field profile

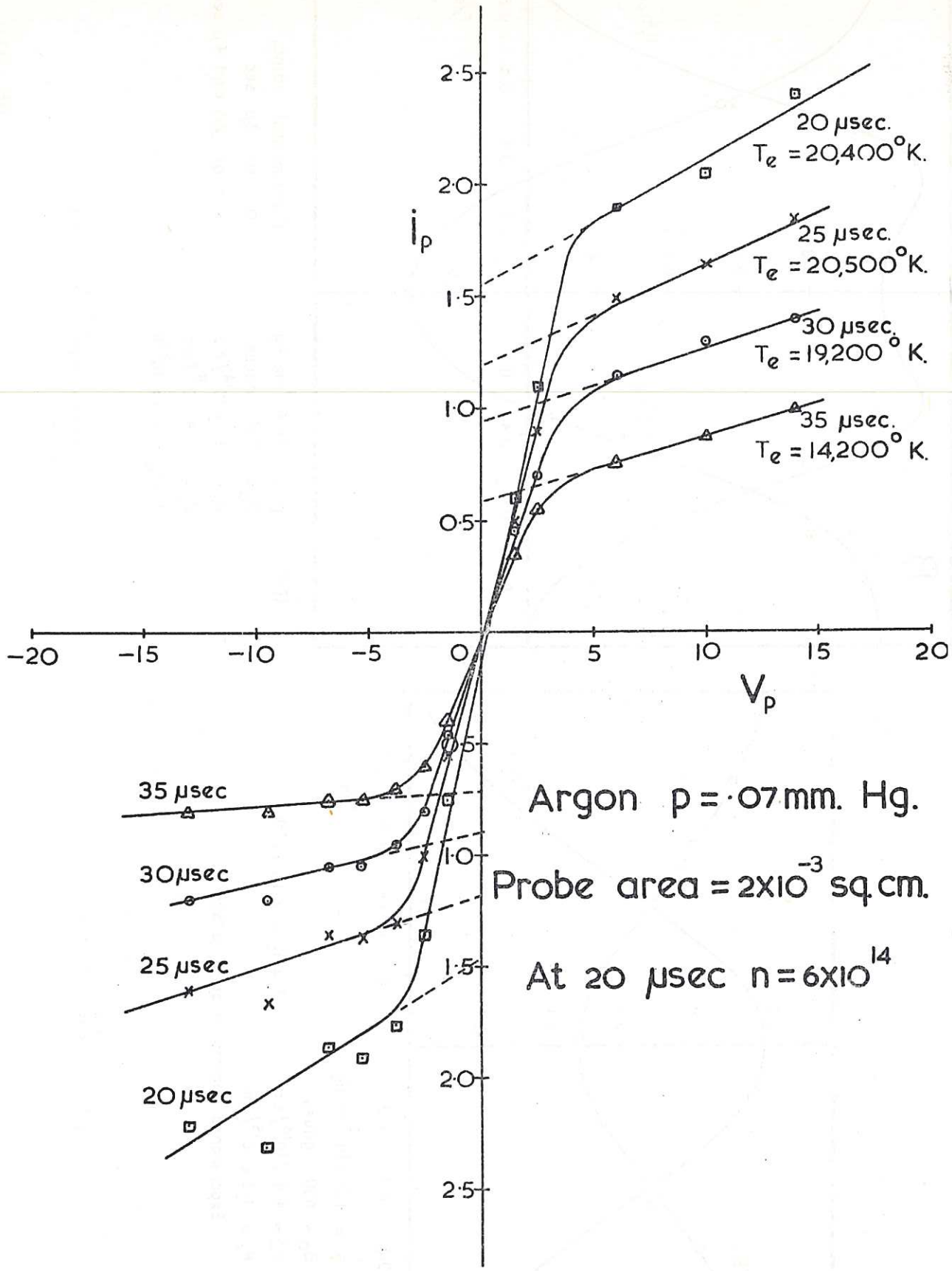

Fig. 7.
Langmuir double probe measurements.

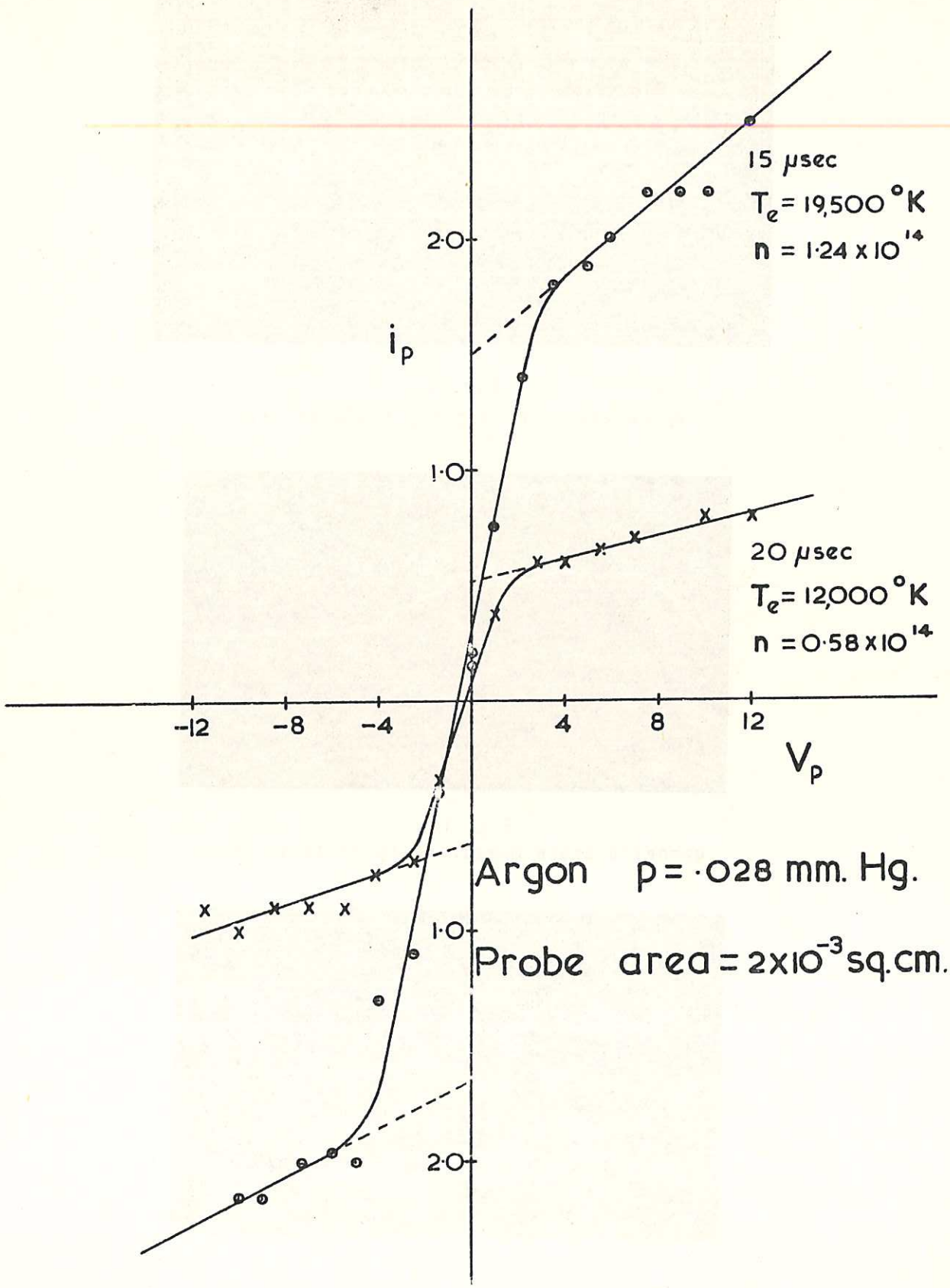

Fig. 8.
Langmuir double probe measurements

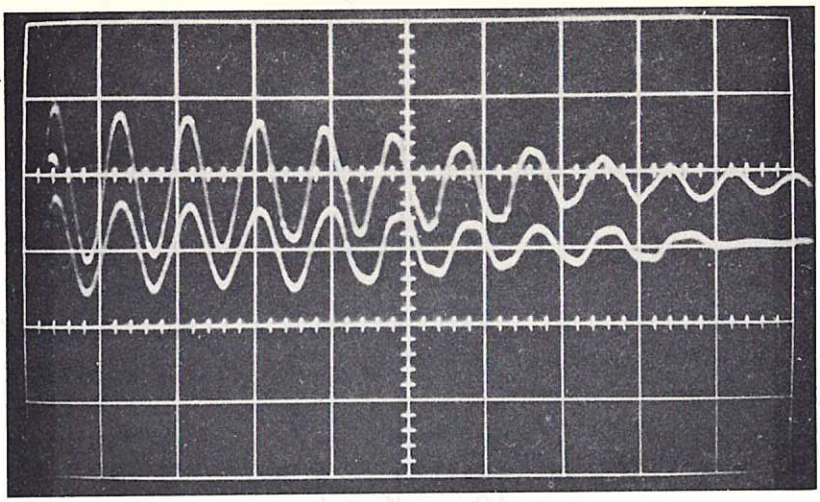

Fig. 9.
Phase shift in rotating field at axis.

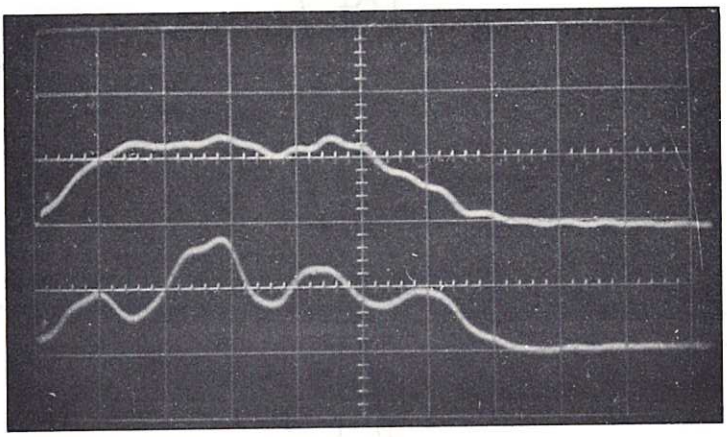

Fig. 10
Magnetic probe measurements of axial field

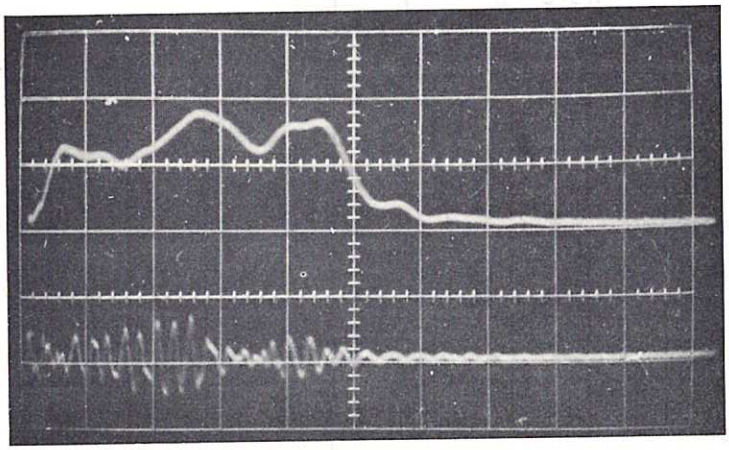

Fig. 11
Second harmonic component of axial field

Available from
HER MAJESTY'S STATIONERY OFFICE
York House, Kingsway, London W.C. 2
423 Oxford Street, London W. 1
13a Castle Street, Edinburgh 2
109 St. Mary Street, Cardiff
39 King Street, Manchester 2
50 Fairfax Street, Bristol 1
2 Edmund Street, Birmingham 3
80 Chichester Street, Belfast
or through any bookseller.

Printed in England

S. O. Code No. 91 - 3 - 11 - 79